JASA ARTICLE

Impact of atmospheric variations on sonic boom loudness over 10 years of simulated flights

Rei Iura,[1] Takahiro Ukai,[1,a)] Hiroshi Yamashita,[2] Bastian Kern,[2] Takashi Misaka,[3] and Shigeru Obayashi[4]

[1]*Department of Mechanical Engineering, Osaka Institute of Technology, 5-16-1 Omiya, Asahi, Osaka, 535-8585, Japan*

[2]*Deutsches Zentrum für Luft- und Raumfahrt, Institut für Physik der Atmosphäre, Oberpfaffenhofen, 82234, Germany*

[3]*Industrial Cyber-Physical Systems Research Center, National Institute of Advanced Industrial Science and Technology, 2-3-26 Aomi, Koto, Tokyo, 135-0064, Japan*

[4]*Institute of Fluid Science, Tohoku University, 2-1-1 Katahira, Aoba, Sendai, 980-8577, Japan*

ABSTRACT:
Relative humidity, temperature, and wind along flight paths from a 10-year simulation are used to investigate the effects of the atmospheric conditions on sonic boom loudness generated by the pseudo-Concorde and a low-boom supersonic aircraft using an acoustic wave propagation tool. Global meteorological conditions are simulated using the chemistry-climate model EMAC with ECMWF reanalysis data. The results show that atmospheric conditions lead to a seasonal variation of the perceived level for a N-wave over 10 years of flights, whereas it is difficult to identify the seasonal variation for the low-boom aircraft because the distribution of perceived levels is widely spread. The dominant effect from atmospheric conditions during acoustic propagation is found for the low-boom aircraft cruising at an altitude of 14.478 km. The molecular relaxation effect is dominant for an overpressure reduction at 10 km but does not impact the pressure waveform below 8 km. At altitudes below 8 km, the thermoviscous absorption exclusively influences the variations in pressure rise time. Moreover, acoustic wave propagation through the turbulent field was simulated at a single location. Even though the acoustic wave passed through the same turbulent field in the summer and winter cases, the loudness on the ground differs between them.
 https://doi.org/10.1121/10.0028375

(Received 11 December 2023; revised 8 July 2024; accepted 13 August 2024; published online 5 September 2024)

[Editor: Philippe Blanc-Benon] Pages: 1529–1542

I. INTRODUCTION

Atmospheric variation is a key factor for loudness due to a sonic boom phenomenon. Shock waves are generated by supersonic transports (SSTs) cruising at supersonic speed and propagate through the atmosphere until it reaches the ground. The representative atmospheric characteristics, such as humidity, temperature, and wind, vary depending on altitude and location and influence the wavefront of the shock wave during the propagation.[1,2] The temperature and relative humidity impact both thermoviscous absorption and molecular relaxation effects on an acoustic pressure waveform. A low temperature increases the rise time of a shock wave, and a low relative humidity decreases its maximum pressure.[3] Acoustic pressure is attenuated by the molecular vibrational excitation of oxygen and nitrogen gases, and the attenuation effects of molecular relaxation depend on the frequency of the pressure waveform.[4,5] Although such thermoviscous absorption and molecular relaxation effects are important to understand the pressure attenuation mechanism, velocity fluctuation in atmospheric turbulence significantly influences the deformation of an acoustic pressure waveform.[6] Previous experimental and numerical studies[7–9] investigated the effects of the turbulence interaction on an acoustic pressure waveform. They showed that the representative effects of turbulence interaction include random variability of the overpressure and pressure rise time, where the overpressure can double in some cases. Such atmospheric effects are important for a sonic boom estimation for the development of the SSTs.

To appropriately estimate sonic boom level on the ground, it is necessary to simulate an acoustic wave passing through various atmospheric conditions. An acoustic wave propagation analysis based on the augmented Burgers equation[10–12] simulates sonic boom propagation with the non-linear and geometrical spreading effects as well as damping effects due to thermoviscous absorption and molecular relaxation. One of the interesting results obtained by the augmented Burgers equation is that all of the molecular relaxation, thermoviscous absorption, and non-linear effects distort the pressure waveform of a non-linear spherically diverging N-wave, increasing the rise time of the waveform.[4] The thickness of a shock wave front related to the pressure rise time influences sonic boom loudness. Doebler *et al.*[13] investigated numerically the boom-carpet of a low-boom aircraft: NASA's X-59 using the PCBoom code, which solves an enhanced Burgers equation along acoustic ray and showed that the boom-carpet width is affected by the atmospheric variation, such as temperature and humidity. The wind effects related to an acoustic ray path become

[a)]Email: takahiro.ukai@oit.ac.jp

important for acoustic propagation through the windy atmosphere. Lonzaga[14] improved the ray path calculation in the PCBoom by incorporating the Doppler shift and convective effect of winds. As mentioned earlier, turbulence interaction with velocity and thermal fluctuations is a key phenomenon, and acoustic propagation through a turbulent field is simulated using several methods based on Khokhlov-Zabolotskaya-Kuznetsov (KZK) equation,[8,15] heterogeneous one-way approximation for the resolution of diffraction (HOWARD) equation,[16–18] and an extended Burgers equation with backscattering effects.[19] A representative previous numerical result using the KZK equation showed that large-scale inhomogeneities in the turbulent field govern primarily the overpressure and arrival time of the acoustic wave.[8] Kanamori *et al.*[18] investigated the effects of turbulence on a low-boom waveform measured during the D-SEND#2 project by JAXA using the sonic boom propagation analysis based on the HOWARD equation. Their results show that the wavefront of the low-boom waveform has a weak distortion compared with that of a conventional N-wave. The HOWARD equation is a better model for the diffraction of waves than the KZK equation. The degree of approximation is the main difference between the parabolic approximation in the KZK and the one-way approximation in the HOWARD. The standard parabolic approximation is valid for the wave direction of low angular, whereas the one-way approximation is valid up to 90 degrees. Nevertheless, both numerical approaches provide sufficient information on the turbulence effects.[8,16–18,20,21] Although there are several approaches to estimate the acoustic propagation, the atmospheric effects can be well investigated using these numerical tools, and such tools enable us to estimate the sonic boom on a flight route with various atmospheric conditions.

A long period of atmospheric variations in location and season impacts the sonic boom characteristic. Leal *et al.*[22] investigated loudness affected by atmospheric variations during short (12 h) and middle (12 month) periods. They showed that relative humidity at a high altitude influences the perceived levels of a low-boom aircraft throughout the year. The sonic boom characteristics based on the atmospheric variations over a longer period were investigated in the literature.[23–26] Blumrich *et al.*[25] investigated focused sonic boom characteristics at the different flight routes over a 10-year period. Their result shows that an effective speed of sound in the troposphere and lower stratosphere perpendicular to the flight direction was an important atmospheric factor for the width of a boom-carpet on the ground. Heimann[26] investigated the boom-carpet variations during 12 years using an acoustic ray tracing simulation and indicated that the boom-carpet is influenced by both wind speed and temperature. Doebler *et al.*[13] used five years of atmospheric profiles at an adjacent location in a range of 60 and 150 km and investigated boom-carpet variations over the contiguous United States of America. They showed that the boom-carpet width of NASA's X-59 aircraft varies depending on season and location. Additionally, its mean width ranged from 42 to 62 km, whereas Heimann[26] showed that the boom-carpet width of a supersonic aircraft varies between 70 and 250 km. This is because these flight conditions and meteorological data differ between them. Salamone[23] investigated loudness variations at different aircraft configurations in atmospheric variations and showed that the low-sonic boom configuration keeps a low loudness. In their atmospheric conditions, it seems a limitation in a period of atmospheric variations and a spatial resolution of meteorological data. The sonic boom characteristics during a long period are affected by the climate conditions, aircraft configurations, and flight conditions, to name a few.

This study focuses on the sonic-boom characteristics between the different aircraft models over the same flight route using a long period of meteorological data. We simulate a meteorological map of the earth over a 10-year period based on simulated meteorological data and investigate sonic boom loudness directly under a flight path. Two types of SST models, namely, the Concorde and a low-boom supersonic aircraft, were used to understand atmospheric effects depending on a sonic boom signature. Even the KZK equation has appropriately captured acoustic propagation through the turbulent field and provides useful information. Thus, the KZK equation is employed to investigate turbulence effects in this study, whereas an augmented Burgers equation is used for acoustic propagation without a turbulent field.

II. NUMERICAL METHODS AND CONDITIONS

A. Sonic boom simulation

To investigate the effects of the atmospheric conditions on the sonic boom propagating through the atmosphere, a propagation analysis tool based on the KZK equation developed by Takeno *et al.*[27] is used. They referred to the articles[28,29] to develop the analysis tool, and the framework of this propagation analysis tool is the same as the Xnoise[10,30] simulating the propagation of the acoustic waves affected by thermoviscous absorption, relaxation, nonlinearity, geometrical spreading, and inhomogeneity of a medium. Additionally, an acoustic propagation through the turbulent field involving velocity fluctuations can be simulated to investigate turbulence effects. The KZK equation is expressed as follows:

$$\frac{\partial p}{\partial z} = \frac{c_0}{2}\int_{-\infty}^{\tau}\left(\frac{\partial^2 p}{\partial x^2}+\frac{\partial^2 p}{\partial y^2}\right)d\tau' + \frac{\beta}{2\rho_0 c_0^3}\frac{\partial p^2}{\partial \tau} + \frac{D}{2c_0^3}\frac{\partial^2 p}{\partial \tau^2} + \sum_i \frac{(\Delta c)_i \tau_i}{c_0^2}\left(1+\tau_i\frac{\partial}{\partial \tau}\right)^{-1}\frac{\partial^2 p}{\partial \tau^2} - \frac{1}{2A}\frac{\partial A}{\partial z}p + \frac{1}{2\rho_0 c_0}\frac{\partial(\rho_0 c_0)}{\partial z}p + \frac{u_z}{c_0^2}\frac{\partial p}{\partial \tau} + \frac{1}{c_0}(\boldsymbol{u}_\perp \cdot \nabla_\perp p), \quad (1)$$

where p is the acoustic pressure; and z and x, y are the propagation coordinate and transverse coordinates, respectively.

$\tau = t - \int dz/c_0$ is the retarded time of the wave. The right-hand side of Eq. (1) represents the various effects on the pressure change along the propagation direction. The first and second terms denote the diffraction and non-linear effects in the acoustic pressure propagation, respectively. β is the coefficient of non-linearity. c_0 and ρ_0 are the ambient speed of sound and the ambient density of the medium, respectively. The third term denotes the thermoviscous absorption effects involving the diffusivity of sound D. The fourth term includes effects of molecular relaxation processes, where τ_i and Δc are the relaxation time and increment in speed of sound. The fifth and sixth terms denote the geometric spreading related to the ray tube area A and the atmospheric stratification, respectively. Note that, while the current propagation tool can simulate the ray path of the acoustic wave below the flight path, it cannot simulate the propagation in the circumferential direction. The last two terms represent the convection effects due to turbulence. u_z is the axial component of the flow, and $\boldsymbol{u}_\perp = (u_x, u_y)$ is the transverse component. The terms expressed as the atmospheric effects on the sonic boom can be individually simulated, thereby transforming into an augmented Burgers equation if the first, seventh, and eighth terms are eliminated. In other words, the augmented Burgers equation is used in the present study when we do not investigate the turbulence effects. We do not simulate the sonic boom–turbulence interaction phenomena along the whole flight path because a huge computational resource is required. Alternatively, acoustic propagation through a turbulent field is simulated at a single ground location (latitude of 53.0555 degrees and longitude of −34.9206 degrees) in a summer (July 15, 2009 at 15:24:00) and a winter (January 15, 2010 at 15:24:00). In the present numerical conditions, the location is not important to investigate the turbulence effect on the sonic boom in winter and summer because the turbulent field is not generated based on meteorological data estimated by the EMAC model. Hence, we chose the middle location of the flight path. The above location is approximately a middle point from New York to London over the flight path. On the other hand, we chose the 15th of July and 15th of January, which are the middle of summer and winter, respectively.

Two types of SST models are employed to investigate the effects of the atmospheric variation on the sonic-boom waveforms. The Concorde, the first aircraft which provided supersonic passenger service, generated a general sonic-boom waveform, namely, an N-wave. The N-wave is suitable for the understanding of basic effects in various atmospheric conditions under a flight route in the past, and its characteristic is useful as the benchmark. Second, a low-boom SST [Low-Boom Concept (LBC)] designed by NASA in the N + 2 program[31] is used for the comparison between general and low sonic-boom concepts. The LBC provides a long rise time sonic-boom waveform, we call it LR-wave in this study. A cruise Mach number for both aircraft are comparable (Table I) and sonic boom characteristics for both can be found in the literature.[32,33] Furthermore, results in this study on the effects of atmospheric variations are useful for future low boom SSTs developments. Figure 1 shows the near-field pressure waveforms for both aircraft. We use a near-field pressure waveform estimated by Ishikawa *et al.*[34] based on a pseudo-Concorde shape[35] for the N-wave generated by the Concorde. Magee *et al.*[32] numerically estimated the near-field pressure waveform of the LBC, and we use the near-field pressure waveform under an ideal design condition (flight Mach number of 1.8 at $h/L = 3.0$ and $CL = 0.1$) for this study. h and CL denote a distance under the body and a lift coefficient, respectively.

TABLE I. The specifications of the Concorde and LBC aircraft.

	Concorde	LBC
Body length L (m)	62.0	61.6
Cruise Mach number M_f	2.0	1.8
Cruise altitude H_c (km)	15.3	14.478
Passenger capacity	100	35-70

B. Climate simulation

We use the chemistry-climate model EMAC 2.54 (ECHAM/MESSy Atmospheric Chemistry)[36,37] to simulate meteorological conditions using the European Centre for Medium-Range Weather Forecasts (ECMWF) ERA-Interim reanalysis data.[38] The atmospheric profiles directly under the flight path are extracted using the air traffic simulation tool AirTraf 2.0.[39] This method provides realistic atmospheric profiles for the simulation period, representing past meteorological conditions on the whole earth, including meteorological observation data. We assume that the

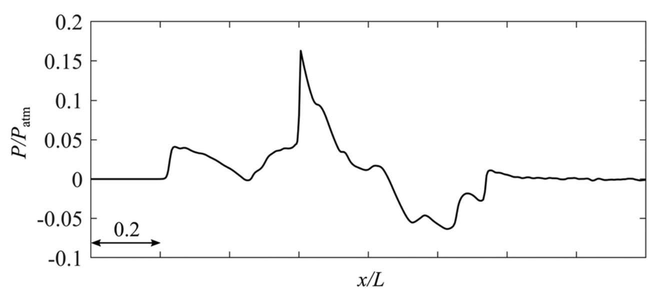

(a)

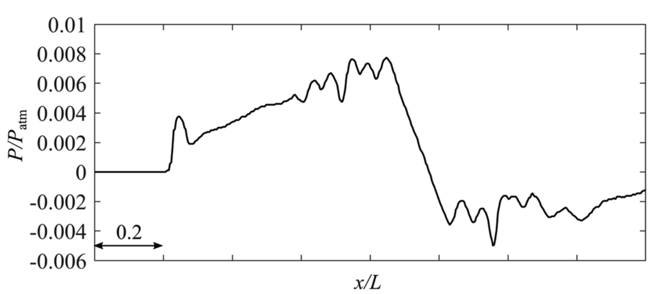

(b)

FIG. 1. The near-field pressure waveforms calculated by computational fluid dynamics in the literature (Refs. 32 and 34). P/P_{atm} denotes pressure change P from an atmospheric pressure P_{atm} around the aircraft. x is the axial location along the aircraft. (a) Pseudo-Concorde ($h/L = 0.5$). (b) LBC ($h/L = 3.0$).

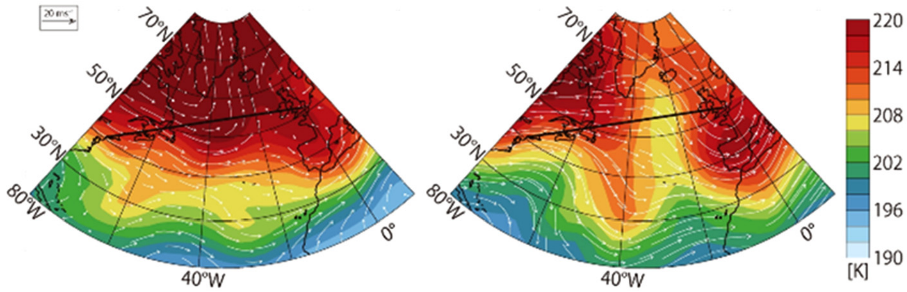

FIG. 2. (Color online) Representative temperatures (contours) with wind vectors at 15.3 km altitude at 10:00 UTC on June 1, 2008 (left) and on December 1, 2008 (right). Thick black solid line denotes the flight route.

Concorde flies from John F. Kennedy Airport at 13:30:00 (UTC) to London Heathrow Airport (i.e., eastbound flight) every day (Fig. 2) on the great circle at $M_f = 2.0$ at an altitude of $H_c = 15.3$ km for the sonic boom estimation. The atmospheric profiles along the altitude H from March 1, 2009 to February 28, 2019 are used in this study (Fig. 3). We do not estimate sonic boom for the takeoff and landing phases because of no sonic boom occurrence. The distance between adjacent positions of the supplied meteorological data is approximately 490 km along the flight path for the supersonic cruise. For estimating the ground sonic boom without turbulence interaction, all meteorological profiles along the flight path over the whole 10 years are used.

According to observed meteorological data,[40] the atmospheric turbulence was assumed as a homogeneous turbulent field. Thus, we use the homogeneous turbulent field for the sonic boom–turbulence interaction in this study. This field is estimated by the turbulence energy spectrum of von Karman and Pao[41] that satisfies well in an inertial subrange up to a dispersion range, and the energy spectrum is expressed as follows:

$$E(k) = \left(\frac{2}{3}\right)^{3/2} \frac{K^{5/2}}{\varepsilon} \frac{(k/k_e)^4}{\left[1 + (k/k_e)^2\right]^{17/6}} \exp\left[-\frac{9}{4}\left(\frac{k}{k_d}\right)^{4/3}\right], \quad (2)$$

where the K is the kinetic energy of the turbulence, and the ε is the turbulence dissipation rate. The k is the wave number of the energy spectrum. The subscripts e and d denote the peak and dissipation wave numbers, respectively. These characteristics are obtained based on the observed atmospheric conditions, and they are set as $K = 0.4\,\mathrm{m^2/s^2}$, $\varepsilon = 1.15 \times 10^{-4}\,\mathrm{m^2/s^3}$, $k_e = 6.28 \times 10^{-3}\,\mathrm{m^{-1}}$, and $k_d = 628\,\mathrm{m^{-1}}$ with reference to a previous study.[42] The turbulence intensity is calculated using the random Fourier mode expressed as follows:[43]

$$\boldsymbol{u}_{\mathbf{t}}(\boldsymbol{y}) = 2\sum_{n=1}^{N} \tilde{u}_{tn} \cos(\boldsymbol{k}_{\mathbf{n}} \cdot \boldsymbol{y} + \psi_n)\boldsymbol{\sigma}_{\mathbf{n}}. \quad (3)$$

The number of Fourier components of $N = 200$ is used; consequently, the homogeneous turbulent field with a velocity fluctuation $V_{rms} = 2.5$ m/s can be generated. For the calculation of the sonic boom propagation in turbulence interaction, a numerical region of $X = 14$ km, $Y = 14$ km, and $Z = 18$ km is used (Fig. 4). An atmospheric boundary layer simulated by Eq. (3) reaches 2 km above the ground. The numerical region is large enough to simulate the diffraction waves due to turbulence interaction. This is because the acoustics pressure field passing through the turbulent region has a lateral extent of 200 m, whereas the calculation region is much larger (14 km) in the horizontal directions. A wide acoustic

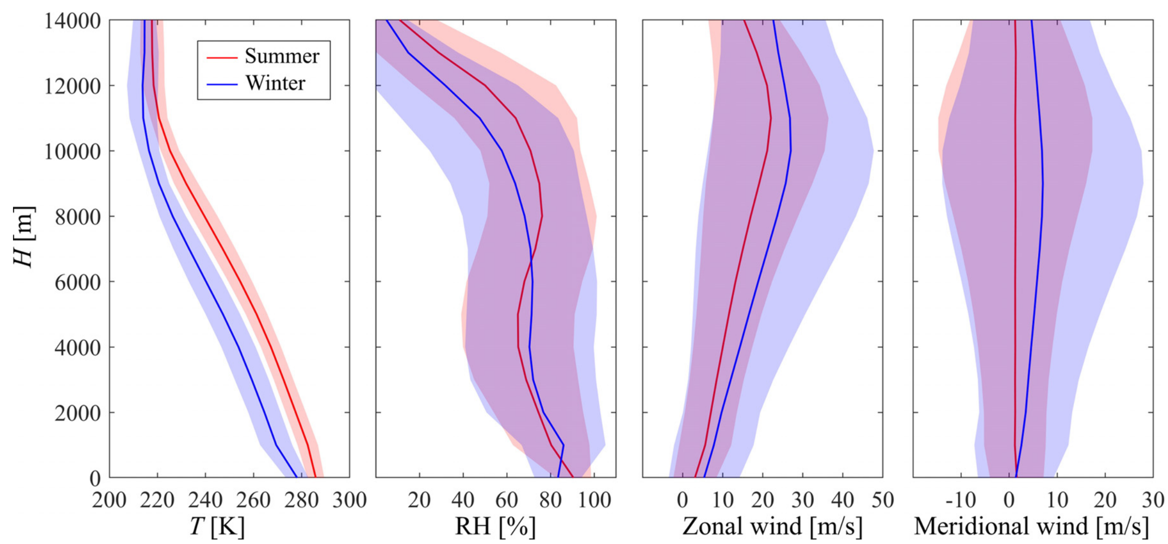

FIG. 3. (Color online) The mean atmospheric profiles over 10 years of flights. Solid line and the translucent edges denote the ensemble mean value and its standard deviation, respectively.

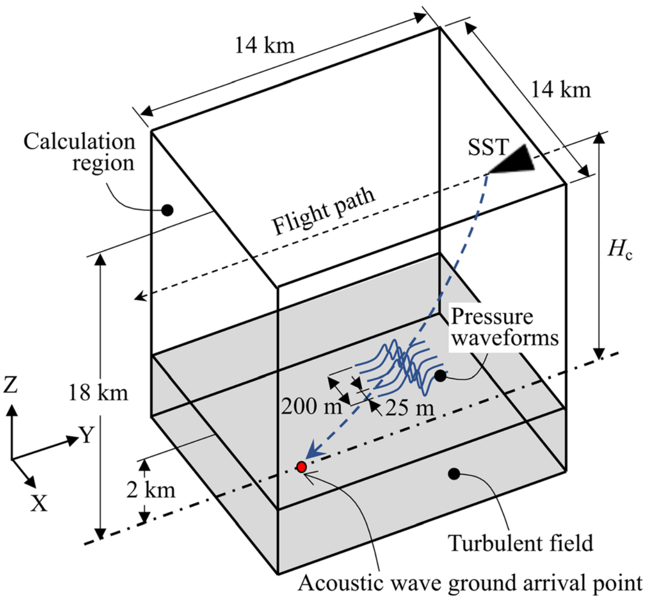

FIG. 4. (Color online) The calculation area for acoustic propagation through the turbulent field.

pressure field with fine spatial resolution provides many sample data for obtaining statistical information, such as average and standard deviation. However, such acoustic pressure fields require a high computational cost to simulate their propagation through the turbulent field. On the basis of a preliminary investigation, the acoustic pressure field of 200 m with spatial resolution of 25 m is suitable so that reasonable sonic boom–turbulence interaction phenomena can be captured with low computational cost. The grid given the velocity component interval in the turbulent field is 100 m in all directions. The duration time of the present pressure waveforms on the ground is approximately 200 ms, resulting in an extent of the acoustics pressure field in the *y*- and *z*-directions of 68 m (= duration time of 200 ms × 340 m/s) and 125 m, respectively. The grid interval for the sonic boom propagation simulation by the KZK equation is 0.1 m until the pressure waveform reaches to the ground. In this study, 60 cases of the turbulent fields are generated to investigate the turbulence effect on the pressure waveform passing through various turbulent fields. However, the turbulence characteristics, namely, the kinetic energy, the turbulence dissipation rate, are constant in the turbulent regions.

Ideally, the turbulence field should be simulated based on meteorological data as well as the various turbulence characteristics. The EMAC model simulated meteorological data at approximately 2.8° × 2.8° horizontal resolution covering the whole earth in the present study. It is difficult to estimate reasonable turbulent fields based on the meteorological data at this rather coarse grid resolution. One of the solutions to create a suitable turbulent field is the improvement of the grid resolution for the simulation; however, the requirement of huge computational resources makes it difficult to simulate. The present simulation cost even at this rather coarse grid resolution was approximately 59 h using a supercomputer at the German Climate Computation Center. Therefore, we focused on the investigation of the turbulence effects between the normal-boom and low-boom signatures using the same homogeneous turbulent field, which is generated based on a previous study.[42] The present investigation is useful to know the turbulence effects between the different pressure waveforms passing through the simulated real atmospheric profile, such as temperature, humidity, and wind.

III. RESULTS AND DISCUSSIONS

A. Sonic boom characteristics over 10 years of flights

The present acoustic wave propagation tool provides overpressure magnitude, which is almost the same as previous results. Figure 5 shows the sonic booms at time passing aircraft over 10 years of flights at the given latitude and longitude on the surface of the earth. Note that the sonic booms passing through the turbulence field created by Eq. (3) are

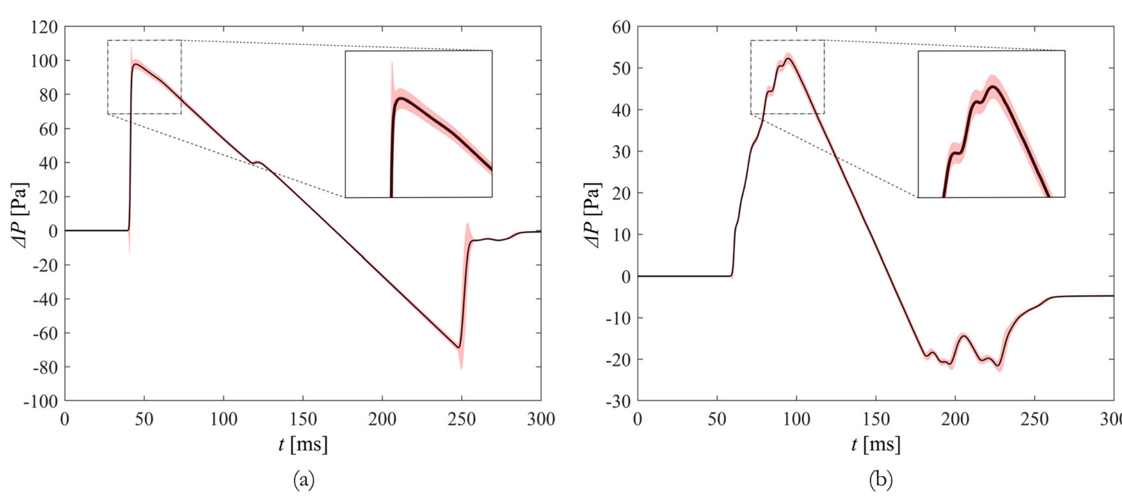

FIG. 5. (Color online) The variation of the pressure waveforms on the ground over 10 years of flights. Solid black line and the translucent red edges denote the ensemble mean pressure waveform and its standard deviation, respectively. Note the different scaling of the *y* axis. (a) Pseudo-Concorde. (b) LBC.

TABLE II. The statistical values of the overpressure and rise time over 10 years of flights.

	$\widehat{\Delta P}$ (Pa)	$\sigma_{\Delta P}$ (Pa)	$\hat{\tau}$ (ms)	σ_{τ} (ms)
Pseudo-Concorde	101	2.90	0.470	0.0706
LBC	52.7	1.31	26.2	0.563

not discussed until Sec. III C. On the basis of arrival time of the sonic boom reaching the ground, mean pressure value at each elapsed time on the pressure waveform was calculated, thereby providing these statistical pressure waveforms shown in Fig. 5. We made the pressure magnitude of a ground pressure waveform double due to the pressure reflection on the ground surface. The present pressure waveform of the LBC [Fig. 5(b)] and its overpressure are in good agreement with the waveform and the overpressure shown in a previous study.[32] Additionally, the acoustic wave propagation tool estimates well the N-wave generated by the pseudo-Concorde [Fig. 5(a)], and its ensemble mean overpressure is $\widehat{\Delta P} = 101$ Pa, which is similar to the previous information.[33,44]

The atmospheric variations influence the pressure change, even though the acoustic waves do not pass through atmospheric turbulence. Table II shows the statistical values obtained from 36 520 ground pressure waveforms over 10 years of flights. The pressure rise time is defined as the elapsed time between 10% and 90% of the overpressure. The front overpressure of the N-wave (pseudo-Concorde) varies in a range of 87.1 and 111 Pa, and its standard deviation is $\sigma_{\Delta P} = 2.90$ Pa. In meteorological data, the relative humidity is widely distributed in a range of 0.328 and 138% below the altitude of 15 km. The relative humidity of more than 100% denotes a supersaturation state. The wide humidity variation might cause the large deformation of the pressure waveforms during sonic boom propagation because the molecular relaxation effects mainly related to the relative humidity strongly attenuates the acoustic pressure.[5] We discuss more the relaxation effects in Sec. III B. Such atmospheric variation influences the low-boom pressure waveform as well. The overpressure of the LR-wave (LBC) does not strongly fluctuate over 10 years of flights compared with the overpressure of the pseudo-Concorde (Table II); however, the pressure rise time of the LBC shows a large standard deviation of $\sigma_{\tau} = 0.563$ ms. The standard deviation of the rise time is a key factor for loudness in the LR-waves.

Both overpressure and rise time are the important characteristics for loudness due to the sonic-boom pressure waveforms. The loudness of the LBC fluctuates largely because of the large standard deviation in the rise time of its pressure waveform. We estimate the perceived level in decibel calculated based on energy in the frequency domain of the pressure waveform, including the overpressure and rise time characteristics. The energy content in each frequency band is obtained via fast Fourier transform analysis on the pressure waveform. On the basis of a sound pressure level related to the energy content, a sound pressure level for the given frequency band is calculated. The sound pressure level is converted into an equivalent loudness for each of the one-third octave frequency bands.[45] Then, an equivalent loudness in sone is analytically estimated, and a total loudness in sone S_t is used to calculate a perceived level, $PL = 32 + 9\log_2(S_t)$. The sone is defined by Stevens as the perceived magnitude of the reference standard 3.15 kHz at the sound pressure level of 32 dB.[46] The full explanation of the calculation procedure is described in the literature.[45,47] The analytical results show that the ensemble mean PL of the pseudo-Concorde is 100 ± 0.460 PLdB, whereas for the LBC it is 80.9 ± 2.10 PLdB. As explained above, the LR-wave has a large standard deviation of the rise time, thereby providing a wide range of perceived levels, even though its variation in the overpressure is small. Despite the large variation in perceived levels, the mean perceived level of the LBC is approximately 19 PLdB lower than that of the pseudo-Concorde, with the maximum $PL = 84.2$ PLdB of the LBC. Therefore, the LBC still retains the advantage of a low sonic-boom aircraft.

The overpressure is significantly fluctuating with the seasons throughout the 10 years and decreases in winter and increases in summer. The overpressure variation over 10 years of flights is shown in Fig. 6 for a deeper understanding of the atmospheric effects. This is because the characteristics of an equivalent loudness are involved in calculating the perceived level, it is complicated for the understanding of the pressure waveform deformed due to the atmospheric effects. The vertical axis in Fig. 6 shows a

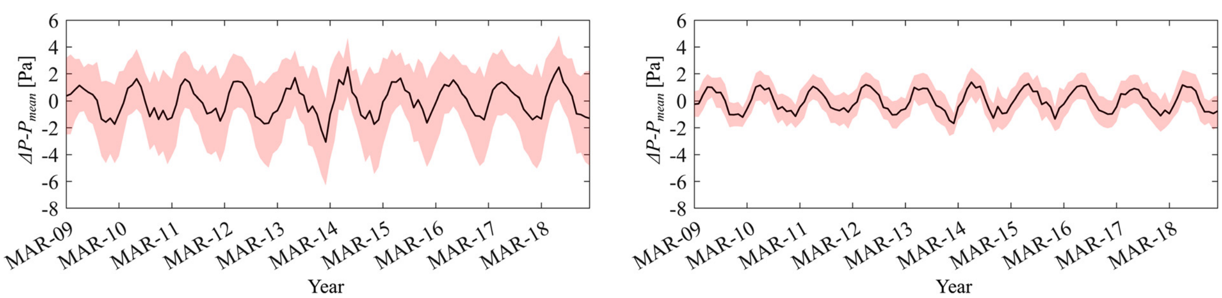

(a) (b)

FIG. 6. (Color online) The seasonal variation of the difference between the overpressure and its mean value over the 10-year period. Solid black line and the translucent red edges denote the ensemble mean pressure difference and its standard deviation, respectively. (a) Pseudo-Concorde. (b) LBC.

TABLE III. The seasonal atmospheric conditions in the altitude range of 0 and 14 000 m over 10 years of flights. The ensemble mean relative humidity $\widehat{\mathrm{RH}}$ and temperature $\widehat{T}$ were obtained in all of the atmospheric profiles under the present 10-year flight routes.

	$\widehat{\mathrm{RH}}$ (%)	$\widehat{T}$ (K)
Summer	64.1 ± 23.4	248 ± 4.48
Winter	59.4 ± 26.3	238 ± 6.01

pressure difference between the overpressure and its mean value over the 10-year period. According to a numerical study by Hodgson,[3] the rise time of a pressure waveform is increased by a low temperature under the assumption of a weak magnitude of the pressure wave, constant surrounding pressure of 1 bar, and constant relative humidity of 50%. Additionally, another numerical investigation showed that a low temperature leads to a large thickness of a shock wave front.[48] On the basis of these results, the overpressure is decreased by the low temperature because the long rise time leads to a general reduction of the overpressure. Additionally, the relative humidity contributes to the seasonal variation as well. This is because a low atmospheric relative humidity enhances the pressure attenuation.[5] This same tendency as that in the variation of the relative humidity with season is shown in Table III. Consequently, most of the overpressures in winter are smaller than those in summer (Fig. 6). However, the overpressure variation for the N-wave in winter is wider than that in summer. The reason would be that the standard deviation of the relative humidity and the temperature in winter is larger than that in summer (Table III).

Loudness of the LBC would not change in season because of the large standard deviation of the perceived level. The perceived level is clearly fluctuating with season for the pseudo-Concorde, and variation is lower in winter and higher in summer [Fig. 7(a)]. As explained at the third paragraph, the perceived level is related to the overpressure; thus, the seasonal tendency is the same as that of the overpressure [Fig. 6(a)]. On the other hand, the seasonal fluctuation of the perceived level would appear for the LBC, but it is not clearly observed because of a wide perceived level distribution [Fig. 7(b)]. Since the pressure rise time is involved in the perceived level, the large standard deviation of the rise time causes the wide perceived level distribution. Although it is not simple relationship between the perceived level and the pressure rise time, we estimate roughly the impact of the overpressure and rise time characteristics to the perceived level based on these standard deviations shown in Table II. The $\sigma_{\Delta P} = 2.90$ Pa of the N-wave (pseudo-Concorde) is approximately two times as large as that of the LR-wave (LBC), and the $\sigma_\tau = 0.0706$ ms of the N-wave is much smaller than that of the LR-wave; thus, the $\sigma_{\Delta P}$ influences dominantly the standard deviation of the perceived level for the pseudo-Concorde. On the other hand, the $\sigma_\tau = 0.563$ ms of the LR-wave is approximately eight times as large as that of the N-wave, thereby providing the larger fluctuation than that of the N-wave. This is because the LBC has the large variation ratio discussed here compared with that of the pseudo-Concorde.

B. Waveform variations during sonic boom propagation

Since the atmospheric conditions vary with altitude, we investigate what the dominant atmospheric features for the deformation of the pressure waveform are. Figure 8 shows the Pearson product-moment correlation coefficient r_p between the atmospheric conditions at each altitude and the overpressure at the ground pressure waveform. The r_p is obtained from 36 520 ground pressure waveforms propagating through each atmospheric profile over 10 years of flights. On the basis of the general threshold for the Pearson's correlation coefficient,[49,50] we assume that $r \geq |0.3|$ has an influence on the pressure waveform. As shown as the green lines in Fig. 8, the correlation coefficients of the atmospheric northward and eastward winds have no correlation with respect to the altitude. Thus, we focus on the effects of the temperature and the relative humidity.

The atmospheric temperature hardly influences the ground overpressure for the acoustic propagation below the flight path. The temperature is dominant at a low altitude during the sonic boom propagation (Fig. 8), whereas the relative humidity effect is more prominent higher altitudes. Here, we discuss the effects of the atmospheric variations on the N-wave (pseudo-Concorde). The effects on the LR-wave (LBC) are discussed in Sec. III C. The temperature and relative humidity are mainly related to the thermoviscous

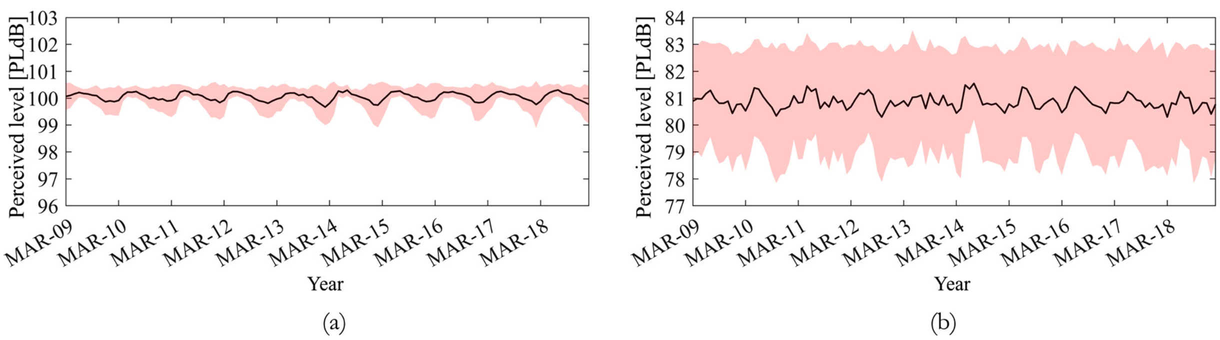

FIG. 7. (Color online) The perceived level in seasonal variation over the 10-year period. Note the different scaling of the y axis. Solid black line and the translucent red edges denote the ensemble mean PL and its standard deviation, respectively. (a) Pseudo-Concorde. (b) LBC.

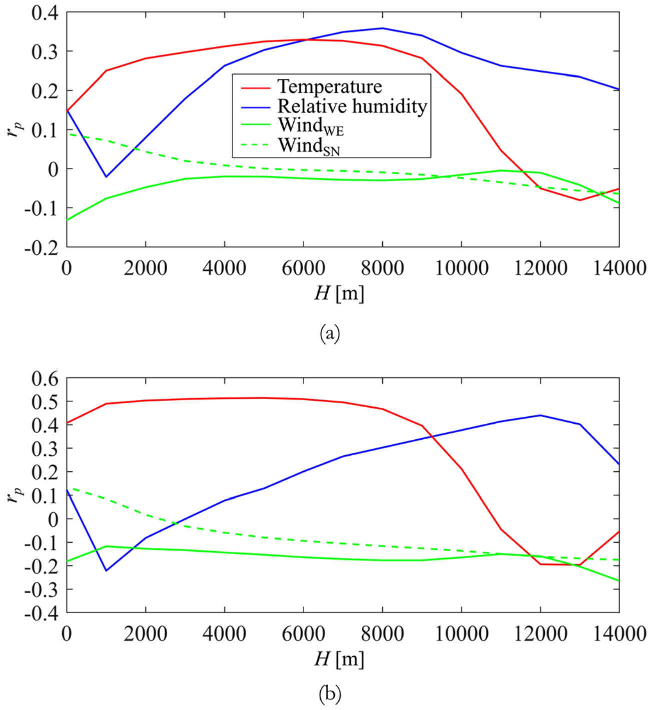

FIG. 8. (Color online) The correlation coefficient between the overpressure of the waveform at ground and atmospheric condition at each altitude. Subscripts WE and SN of the wind denote the flow direction: west-east and south-north, respectively. (a) Pseudo-Concorde. (b) LBC.

absorption and molecular relaxation effects, respectively. To investigate the impact of those effects over 10 years of flights, the sonic boom propagation affected by each effect was separately simulated. Additionally, only two acoustic characteristics, i.e., the non-linear effects and geometric expansion, were calculated during the sonic boom propagation for the comparison of the pressure waveforms due to the thermoviscous absorption and molecular relaxation effects. Consequently, the ground overpressure by the thermoviscous absorption and molecular relaxation effects are 123 ± 3.95 Pa and 101 ± 2.92 Pa, respectively. On the other hand, the ground overpressure without the effects of the atmospheric variations shows 124 Pa. Thus, the thermoviscous absorption effect hardly influences the pressure change. Although the thermoviscous absorption effect is dominant at low altitudes during sonic boom propagation, the pressure reduction by thermoviscous absorption is minor. The present numerical investigation is limited to acoustic propagation in one direction. Hence, it shows that the atmospheric temperature hardly reduces the ground overpressure below the flight path, whereas the previous results showed that the wind and temperature affect the boom-carpet and shadow zone.[13,24]

The features, in which the molecular relaxation effects due to the relative humidity are dominant at the relatively high altitude, can be explained based on a frequency analysis. Pressure attenuation due to the molecular relaxation is strong in both high- and medium-frequency bands in the pressure waveform.[5] Hence, we investigated the frequency characteristics changing along the altitude. The power spectral densities of the present pressure waveforms at altitudes of 2000, 8000, and 14 000 m, were calculated using the fast Fourier transform analysis, and then the energy spectral densities (ESD) = power spectral density × the duration time of analysis data were obtained. A total of 120 pressure waveforms (= a pressure waveform each month × 10 years) at each altitude were used to obtain an ensemble mean. The ensemble mean ESDs at each frequency are shown in Fig. 9. The N-wave in the vicinity of the aircraft (altitude of 14 000 m) contains more high- and medium-frequency bands than that at other altitudes [Fig. 9(a)]. This is because the shock waves generated from various parts of an aircraft are propagated and integrated, which results in the pressure waveform consisting of the shock waves with the high-frequency bands. Therefore, the molecular relaxation effect is enhanced at the higher altitudes, but the correlation coefficient is slightly smaller at the altitude of 14 000 m [Fig. 8(a)]. We discuss the reason for small r_p at 14 000 m in the following paragraph. The relative humidity is strongly related to the pressure reduction in a range of approximately 5000 and 10 000 m in altitude [Fig. 8(a)]. The reason for the large correlation coefficient in this region is that the pressure

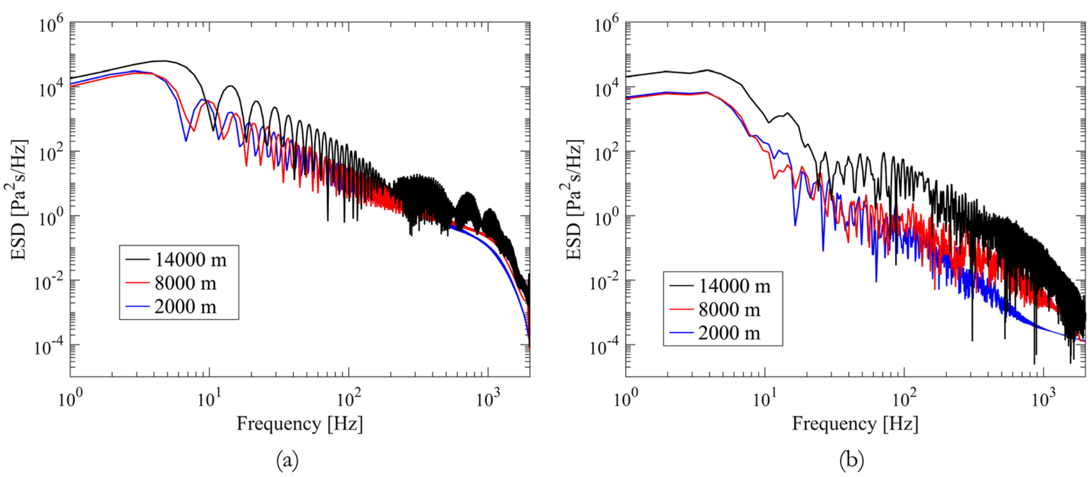

FIG. 9. (Color online) The ensemble mean ESD of the pressure waveform at the altitudes of 2000, 8000, and 14 000 m. (a) Pseudo-Concorde. (b) LBC.

waveform still consists of the high- and medium-frequency bands at 8000 m [Fig. 9(a)]. On the other hand, the ESD at the altitude of 2000 m is relatively small in the high-frequency band [Fig. 9(a)] and has a small r_p [Fig. 8(a)]. Thus, the pressure attenuation due to molecular relaxation has no strong effect at the altitude of 2000 m.

The reason for the weak molecular relaxation effect in an altitude range of approximately 10 000 and 14 000 m is that a non-linear effect is dominant in the vicinity of the pseudo-Concorde. Figure 10 shows the pressure reduction ratio $(d(\Delta P)/dz)_j = (\Delta P_{j+1} - \Delta P_{j-1})/2\,dz$ along propagation direction z based on the acoustic wave propagation analysis applying only non-linear effects and geometric expansion. The subscript j indicates a grid point at an arbitrary altitude. The linearity of the waveform can be identified based on the reduction ratio $d(\Delta P)/dz$. A large reduction ratio indicates non-linearity. In the range of approximately 8000 and 14 000 m, the overpressure of the N-wave decreases non-linearity, whereas the pressure changes weak non-linearity in the range of approximately 0 and 8000 m, where the reduction ratio is relatively constant (Fig. 10). It deduces that pressure waveform attenuated by the molecular relaxation effects is strongly deformed by the non-linear effects in the range of approximately 8000 and 14 000 m. Consequently, we cannot identify molecular relaxation effects in this region for the N-wave.

C. Atmospheric effects on the LR-wave

The contribution of the molecular relaxation effect differs between the N-wave and the LR-wave. As shown in Fig. 8, the correlation coefficient of the relative humidity is large at the relatively high altitude for the LR-wave, and its peak appears at the altitude of 12 000 m, whereas the coefficient peak of the N-wave appears at 8000 m. The reason for the different coefficient peaks between the N- and LR-waves is that the non-linear effect preventing the molecular relaxation effect would depend on the frequency characteristics of the waveform and overpressure magnitude. The pressure reduction ratio shows weak non-linearity below the altitude of approximately 10 000 m for the LR-wave (Fig. 10). Additionally, the reduction ratio of the LR-wave more than 9000 m in altitude is smaller than that of the N-wave. Hence, the non-linear effect on the LR-wave is not strong in the vicinity of the LBC, and the molecular relaxation effect is dominant at a relatively higher altitude for the LR-wave compared with the N-wave.

The molecular relaxation effect for the LR-wave is not important at a middle/low altitude. The LR-wave has a lower magnitude in the high-frequency bands at the altitudes of 2000 and 8000 m compared with that of the N-wave (Fig. 9). The LR-wave shows a relatively smooth waveform consisting of low- and medium-frequency components. Since the molecular relaxation effects are enhanced in both high- and medium-frequency bands,[5] the low magnitude in the high-frequency bands results in weak contribution to the pressure reduction. Therefore, the weak correlation coefficient of the relative humidity appears below the altitude of 7000 m for the LR-wave [Fig. 8(b)].

Let us focus the molecular relaxation effect on the rise time of the LR-wave. Figure 11 shows the Pearson's correlation coefficient r_τ between the atmospheric conditions and the pressure rise time of the LR-wave at the ground. The r_τ of the relative humidity is small below the altitude of 10 000 m, whereas it becomes large above the altitude of 10 000 m. Although the non-linear effect prevents the molecular relaxation effect acting on the overpressure reduction, its impact on the pressure rise time is not clearly seen in the present results. At least, the molecular relaxation effect significantly influences the pressure rise time at the high altitude.

The temperature variation does not strongly influence the overpressure reduction for the LR-wave; however, it influences the pressure rise time. Overpressure reduction due to the thermoviscous absorption and molecular relaxation effects for the LR-wave was investigated, and the

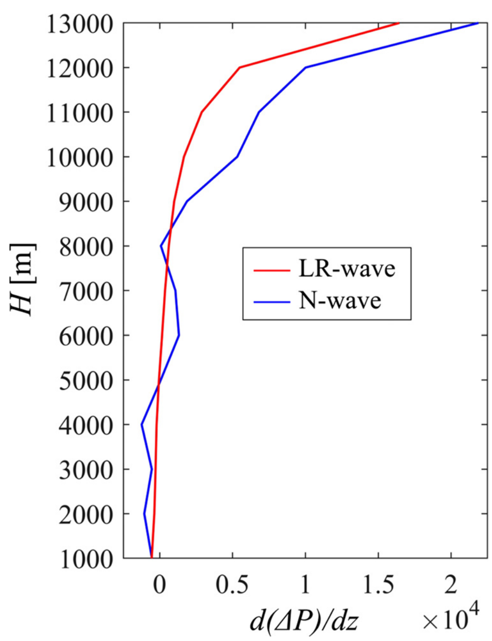

FIG. 10. (Color online) The representative pressure reduction ratio related to the linearity of the sonic boom propagation along the altitude.

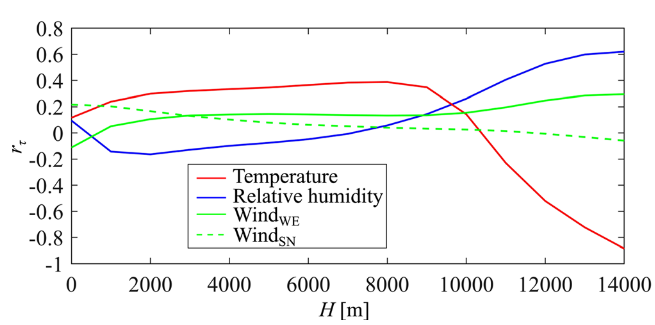

FIG. 11. (Color online) The correlation coefficient between the rise time at the ground pressure waveform and atmospheric condition at each altitude for the LBC.

TABLE IV. The rise time and overpressure variations due to the thermoviscous absorption and molecular relaxation effects over 10 years of flights for the LR-wave. The $\widehat{\Delta P}$ and $\hat{\tau}$ obtained in the conditions of both non-linearity and geometric expansion do not denote mean value and are the same as that of all locations.

The atmospheric effects	$\widehat{\Delta P}$ (Pa)	$\hat{\tau}$ (ms)
Non-linearity and geometric expansion	56.9	26.1
Thermoviscous absorption	57.6 ± 1.36	26.1 ± 0.616
Molecular relaxation	52.8 ± 1.31	26.2 ± 0.563

overpressure without the atmospheric effects was calculated as well. Consequently, their pressure differences of the overpressure without the atmospheric effects are 0.7 and −4.1 Pa, respectively (Table IV). Note that the calculation procedure is the same as that of the N-wave described in Sec. III B. The relative humidity is more impactful on the overpressure reduction, even though the r_p of the temperature is large at the low altitudes [Fig. 8(b)]. However, the thermoviscous absorption leads to variation in the rise time (Table IV). The ensemble mean rise time hardly changes due to the atmospheric variations, but a relatively large standard deviation appears ($\sigma_\tau = 0.616$ ms, shown in Table IV) by the thermoviscous absorption effect. As shown in Fig. 11, the r_τ is large at all altitudes, but its contribution to each altitude is unclear, and further investigations are necessary for understanding it. Although the thermoviscous absorption effect is related to both overpressure and the rise time at the low altitude, the effect strongly influences only the rise time variation.

On the basis of the discussion earlier, the dominant atmospheric effects on the LR-wave are summarized in Fig. 12. The LR-wave is strongly dominated by the non-linear effect in the vicinity of the LBC, but the non-linear effect acting on the overpressure reduction becomes weak once the sonic boom propagates to the altitude of 10 000 m (Fig. 12, black box). In the altitude range of 12 000 and 8000 m, the molecular relaxation effect due to the relative humidity is dominant for the overpressure reduction (Fig.

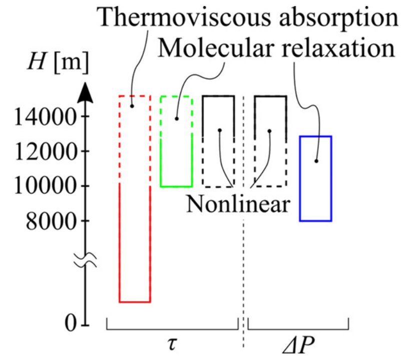

FIG. 12. (Color online) The dominant atmospheric conditions for the pressure variations of the LBC. Dashed line denotes an obscure area in each effect.

12, blue box), and it does not impact the pressure waveform any more at altitudes below 8000 m. Instead of the molecular relaxation effect below the altitude of 8000 m, the thermoviscous absorption effect due to the temperature is dominant but affects only the variation of the pressure rise time (red box shown in Fig. 12).

D. Effects of atmosphere turbulence

Our tool provides the similar results reported in the literature.[51–53] The N-wave transforms into rounded or spiked waveforms due to turbulence interaction [Fig. 13(a)]. The spiked waveform shown as a red line in Fig. 13(a) presents a maximum overpressure due to turbulence interaction in the 1080 pressure waveforms, whereas the round-shaped waveform indicates a minimum overpressure. These pressure waveforms are observed in several flight tests during the investigations of the turbulence interaction for sonic booms.[51–53] To investigate an overpressure distribution due to turbulence interaction, we calculated the histogram of the overpressure for the summer case (Fig. 14). The overpressure by the turbulence effect is normalized by that of the non-turbulence. The bin widths in Fig. 14 were set to $(\Delta P_{\mathrm{turb}}/\Delta P_{\mathrm{no}})_{\max} - (\Delta P_{\mathrm{turb}}/\Delta P_{\mathrm{no}})_{\min} / \sqrt{n} \approx 0.10$ and 0.03

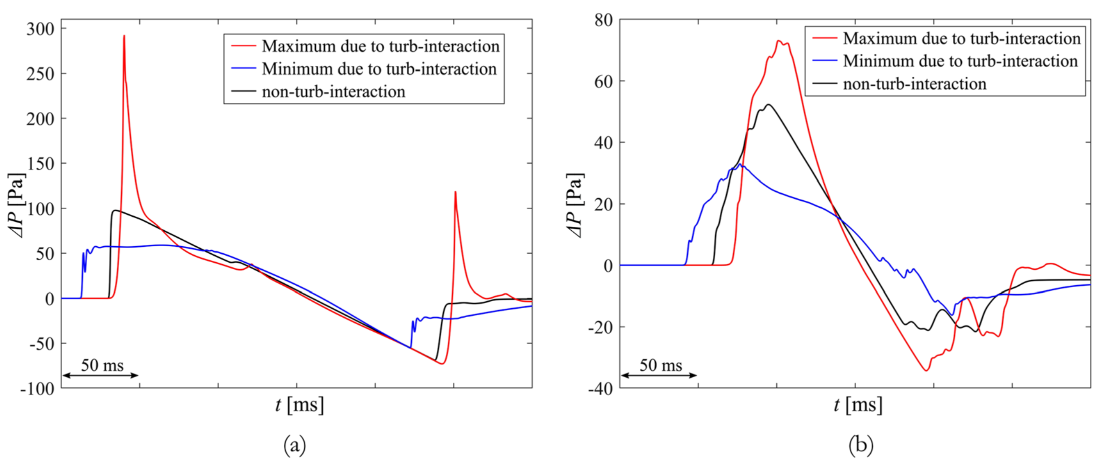

FIG. 13. (Color online) The pressure waveform distorted due to turbulence interaction in both summer and winter cases. (a) Pseudo-Concorde. (b) LBC.

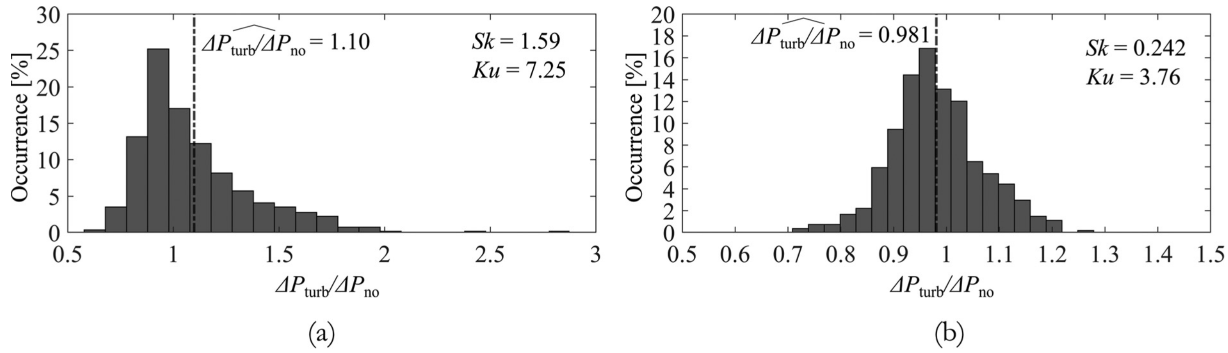

FIG. 14. Histogram of the normalized overpressure in the summer case. The bin size of 0.10 and 0.03 for these histograms of the pseudo-Concorde and the LBC, respectively. Vertical black dot-dashed line denotes the ensemble mean normalized overpressure. (a) Pseudo-Concorde. (b) LBC.

for the pseudo-Concorde and the LBC, respectively. $n = 540$ is the number of the pressure waveforms in the range of the maximum normalized overpressure $(\Delta P_{\rm turb}/\Delta P_{\rm no})_{\rm max}$ and the minimum one $(\Delta P_{\rm turb}/\Delta P_{\rm no})_{\rm min}$ in each season. The subscripts *turb* and *no* denote turbulence interaction and non-turbulence interaction, respectively. The histogram of the N-wave shows a right-skewed distribution, which is comparable to those of previous studies from a flight test.[54] In a previous numerical study by Yuldashev *et al.*,[21] the influences of turbulence intensity on the overpressure of a N-wave were investigated using the KZK-type equation. One of their results indicated that the probability density of the overpressure in a linear propagation case showed a wide right-skewed distribution at long acoustic propagation. The previous experimental and numerical results in a nonlinear propagation case indicated the wide right-skewed distribution of the overpressure.[8,55] Additionally, previous studies[51,56] indicated that a sonic boom loudness change due to turbulence interaction is well approximated by a normal distribution. Although we discuss deeply turbulence effects on the loudness in the following paragraph, the present results show the same tendency. Therefore, the numerical conditions as well as the sonic boom propagation tool provide the reasonable results for the simulation of sonic boom–turbulence interaction. Despite such results, the homogeneous turbulent field does not perfectly simulate a real turbulence field in an atmospheric boundary layer; thus, an inhomogeneous turbulent field provided by the simulated meteorological data is required for further investigations.

Turbulence interaction causes the deformation of the LR-wave as well, but its overpressure magnitude does not vary widely compared with that of the N-wave. The ground overpressure magnitude of the N-wave varies in a range of 58.9 and 292 Pa in the summer and winter cases, namely, the overpressure variation of 233 Pa (= 292 − 58.9 Pa). The overpressure of the N-wave increases to a maximum of 191 Pa from the pressure waveform of non-turbulence interaction in the summer case. On the other hand, for the LR-wave, the maximal overpressure difference is 18.6 Pa between the cases with and without turbulence interaction. Moreover, the overpressure variation between maximum and minimum is 34.5 Pa in the summer case, which results in overpressure variation of approximately 0.148 (= 34.5 Pa / 233 Pa) times smaller than that of the N-wave. Additionally, the overpressure is not dramatically increased due to turbulence interaction for the LR-wave. As shown in Fig. 14(a), a large overpressure magnitude, which is more than double as large as that of the pressure waveform without turbulence interaction, appears only in very few percentages of occurrence, and the normalized overpressure $\Delta P_{\rm turb}/\Delta P_{\rm no}$ distributes widely on the larger end. On the other hand, the normalized overpressure of the LR-wave looks relatively like a normal distribution [Fig. 14(b)], and there is not double normalized overpressure which appears for the N-wave. The maximum normalized overpressure of $\Delta P_{\rm turb}/\Delta P_{\rm no} = 1.34$ appears for the LBC.

Although the effect of turbulence interaction on the overpressure differs between the N- and LR-waves, the turbulence effect is similar between their perceived level values. As shown in Fig. 14, they are distributed in a non-normal distribution. To quantitatively investigate their features, the skewness *Sk* and the kurtosis *Ku* were calculated as follows:

$$Sk = \frac{\frac{1}{n}\sum_{i=1}^{n}(x_i - \widehat{x})^3}{s^3}, \quad Ku = \frac{\frac{1}{n}\sum_{i=1}^{n}(x_i - \widehat{x})^4}{s^4}, \tag{4}$$

where $s = \sqrt{(1/n)\sum_{i=1}^{n}(x_i - \widehat{x})^2}$ and $x = \Delta P_{\rm turb}/\Delta P_{\rm no}$. The circumflex denotes the ensemble mean. Positive and negative *Sk* values denote a distribution deviation to the right and left sides, respectively, and $Sk = 0$ means a normal distribution. A normal distribution appears at $Ku = 3$, and the distribution becomes a round peak when *Ku* is more than 3. Consequently, both $Sk = 1.59$ and $Ku = 7.25$ for the N-wave show a non-normal distribution, whereas the values in the LR-wave fit a normal distribution better, but it might be a non-normal distribution. Since turbulence interaction leads to the wave deformation including rise time variation,[51] it is suitable to evaluate the turbulence effects based on the perceived level on the histogram (Fig. 15). Note that the bin

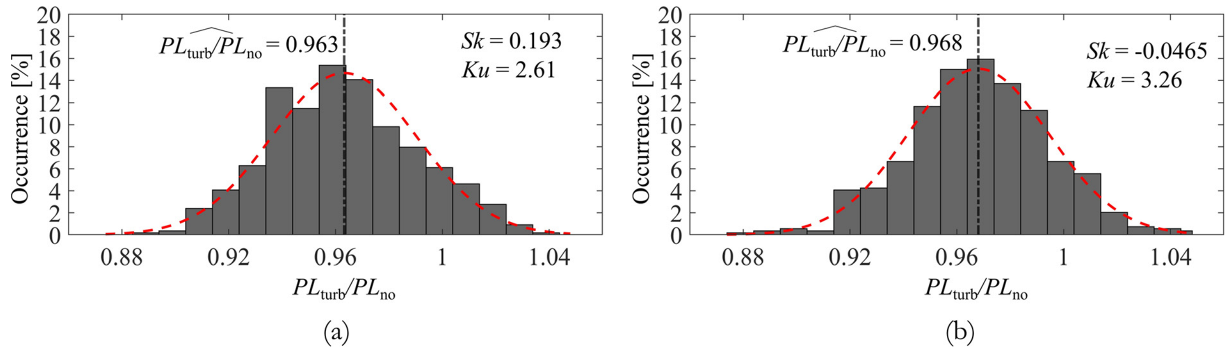

FIG. 15. (Color online) Histogram of the normalized perceived level in the summer case. The bin size is 0.01 in both histograms. Red dashed and vertical black dot-dashed lines denote the normal distribution curve and the ensemble mean normalized perceived level, respectively. (a) Pseudo-Concorde. (b) LBC.

widths in Fig. 15 are suitably adjusted in each histogram. Both histograms of the N- and LR-waves capture well the turbulence effects because the distribution shape and the features (*Sk* and *Ku*) indicate a normal distribution. The mean normalized perceived level for the N- and LR-waves is $\widehat{PL_{turb}/PL_{no}} = 0.963 \pm 0.0272$ and 0.968 ± 0.0265 in the summer case, respectively. The mean normalized perceived level in the winter case shows the same feature. It deduces that turbulence interaction does not significantly change the perceived level compared with the overpressure, and the distribution of the *PL* is similar between the N- and LR-waves.

There is the meteorological impact on the overpressure variation due to turbulence interaction, but the turbulence effects on the perceived level hardly change even at the different seasons. Figure 16 shows the atmospheric profiles for the simulation of sonic boom–turbulence interaction. Although representative meteorological data were employed in each summer (July 15, 2009 at 15:24:00) and winter (January 15, 2010 at 15:24:00), the atmospheric conditions capture the seasonal features. The mean in altitude of the temperature and relative humidity are high in summer and low in winter, respectively. For sonic boom–turbulence interaction, the acoustic wave passed through such an atmosphere interacts with the turbulent field; thus, the pressure waveform before the turbulence interaction varies depending on each atmospheric condition in the summer and winter cases. On the basis of the results discussed in Sec. III A, both low temperature and low relative humidity contribute to the overpressure reduction (see Fig. 6 as well). Note that these features are obtained in the non-turbulence interaction case. In the case of the turbulence interaction, the normalized overpressure $\widehat{\Delta P_{turb}/\Delta P_{no}}$ of the LR-wave decreases in the winter case, and the standard deviation is larger than that of the summer case (Table V). It seems that these characteristics are the same tendency as the overpressure fluctuation in season. Hence, there is a possibility that the low overpressure waveform before penetrating the turbulent field enhances the pressure reduction due to turbulence interaction. A previous result supports such a presumption. They indicated that a low-pressure magnitude enhances pressure reduction

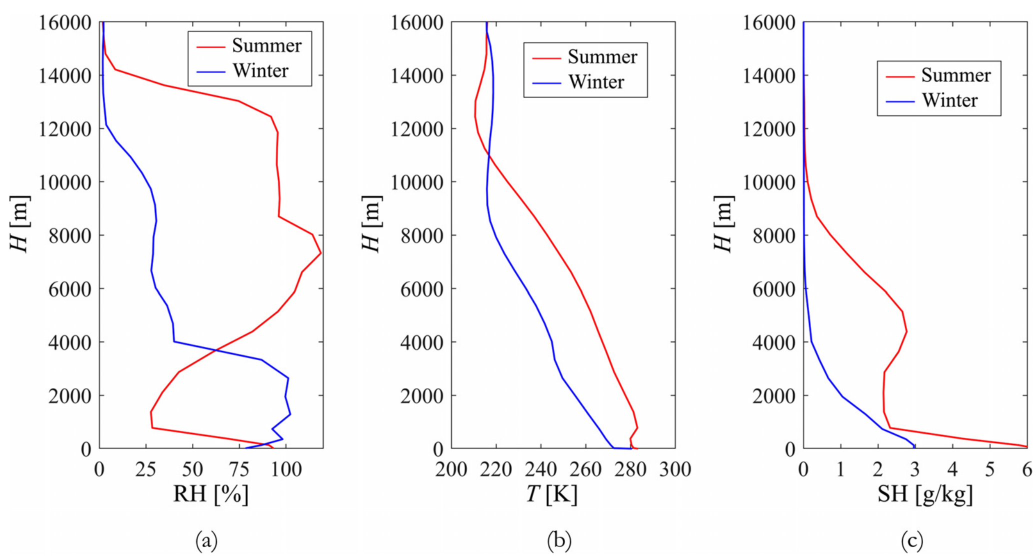

FIG. 16. (Color online) The atmospheric profiles at the location in each summer (July 15, 2009 at 15:24:00) and winter (January 15, 2010 at 15:24:00) case. (a) Relative humidity. (b) Temperature. (c) Specific humidity.

TABLE V. The difference of the ensemble mean normalized features, namely, perceived level and the overpressure, between the summer and winter cases for the LR-wave (LBC).

	$\widehat{\Delta P_{turb}/\Delta P_{no}}$	$\widehat{PL_{turb}/PL_{no}}$
Summer case (July 15, 2009 at 15:24:00)	0.981 ± 0.0881	0.968 ± 0.0265
Winter case (January 15, 2010 at 15:24:00)	0.976 ± 0.103	0.969 ± 0.0264

when an acoustic wave with a weak overpressure passes through a turbulent field.[21] On the other hand, the normalized perceived level hardly changes between the summer and winter cases (Table V) because the seasonal fluctuation is weak in perceived level [Fig. 7(b)].

IV. CONCLUSION

The effects of the atmospheric conditions on sonic boom loudness generated by the pseudo-Concorde and the LBC were investigated using supersonic flights from John F. Kennedy Airport to London Heathrow Airport for 10 years. Global meteorological condition was simulated by using the EMAC model with ECMWF reanalysis data; the supersonic flights were simulated by AirTraf, and the atmospheric profiles directly under the flight path were extracted. The distance between adjacent positions supplied meteorological data were approximately 490 km along the flight path during supersonic cruise. The sonic boom propagation through the representative atmospheric conditions, i.e., relative humidity, temperature, and wind, was simulated using the sonic boom propagation tool based on the KZK equation. Turbulence interaction with the sonic boom was simulated at the single location in winter and summer.

The results for the sonic boom propagation without turbulent interaction showed that the overpressure of the N-wave significantly fluctuates with the season throughout the 10 years, especially the overpressure decreases in winter and increases in summer. The N-wave shows the seasonal variation of the perceived level as well. On the other hand, the perceived level did not strongly seasonally fluctuate for the LR-wave because the rise time of its waveform has the large standard deviation over 10 years of flights. The dominant effect from atmospheric conditions during the sonic boom propagation to the ground was found for the low-boom supersonic aircraft; consequently, the molecular relaxation effect is dominant for the overpressure reduction at 10 000 m. It does not impact the overpressure at the middle altitudes from 8000 m and below. Instead of the molecular relaxation effect below the middle altitude, the thermoviscous absorption effect is dominant but affects only the variation of the pressure rise time.

The turbulence interaction was investigated using meteorological data at the single location in each summer and winter. The sonic boom passed through the same turbulent field in the summer and winter cases to mainly clarify the meteorological impact during the sonic boom–turbulence interaction. Both low temperature and low relative humidity contribute to the overpressure reduction of the LR-wave due to sonic boom–turbulence interaction. There is a possibility that the low overpressure waveform before penetrating the turbulent field enhances the pressure reduction due to turbulence interaction. Ideally, the turbulence field should be simulated based on meteorological data as well as the various turbulence characteristics. Hence, further investigations are necessary to clarify the pressure waveform variation due to the turbulence interaction at several locations and seasons because a turbulent field varies depending on location and time of the season.

ACKNOWLEDGMENTS

The project Sonicboom Evaluation in Realistic Atmospheres is supported by Collaborative Research Project No. J22I036 of the Institute of Fluid Science, Tohoku University. The near-field pressure waveform of pseudo-Concorde was provided by courtesy of JAXA.

AUTHOR DECLARATIONS

Conflict of Interest

The authors declare that they have no conflict of interest.

DATA AVAILABILITY

The ground pressure waveforms passed through present meteorological data are available from the corresponding author upon reasonable request.

[1] E. J. Kane, "Some effect of the atmosphere on sonic boom," in *Proceedings of Sonic Boom Research, NASA SP-147* (1967).
[2] H. E. Bass and R. Raspet, "Vibrational relaxation effects on the atmospheric attenuation and rise times of explosion waves," J. Acoust. Soc. Am. **64**, 1208–1210 (1978).
[3] J. P. Hodgson, "Vibrational relaxation effects in weak shock waves in air and the structure of sonic bangs," J. Fluid Mech. **58**(1), 187–196 (1973).
[4] P. V. Yuldashev, M. V. Averiyanov, V. A. Khokhlova, S. Ollivier, and P. Blanc-Benon, "Nonlinear spherically divergent shock waves propagating in a relaxing medium," Acoust. Phys. **54**(1), 32–41 (2008).
[5] K. Hatanaka and T. Saito, "Numerical analysis of weak shock attenuation resulting from molecular vibrational relaxation," Shock Waves **21**, 121–129 (2011).
[6] I. E. Gurrick and D. J. Maglieri, "A summary of results on variations associated with atmospheric conditions," NASA Technical Note, TN D-4588 (1968).
[7] A. D. Pierce and D. J. Maglieri, "Effects of atmospheric irregularities on sonic-boom propagation," J. Acoust. Soc. Am. **51**, 702–721 (1972).
[8] M. Averiyanov, P. Blanc-Benon, R. O. Cleveland, and V. Khokhlova, "Nonlinear and diffraction effects in propagation of N-waves in randomly inhomogeneous moving media," J. Acoust. Soc. Am. **129**(4), 1760–1772 (2011).
[9] B. Lipkens and D. T. Blackstock, "Model experiment to study sonic boom propagation though turbulence. I: General results," J. Acoust. Soc. Am. **103**(1), 148–158 (1998).
[10] M. Yamamoto, A. Hashimoto, T. Aoyama, and T. Sakai, "A unified approach to an augmented Burgers equation for the propagation of sonic booms," J. Acoust. Soc. Am. **137**(4), 1857–1866 (2015).
[11] S. K. Rallabhandi, "Advanced sonic boom prediction using the augmented Burgers equation," J. Aircr. **48**(4), 1245–1253 (2011).
[12] W. Li and S. Rallabhandi, "Inverse design of low-boom supersonic concepts using reversed equivalent-area targets," J. Aircr. **51**(1), 29–36 (2014).

[13]W. J. Doebler, S. R. Wilson, A. Loubeau, and V. W. Sparrow, "Simulation and regression modeling of NASA's X-59 low-boom carpets across America," J. Aircr. **60**(2), 509–520 (2023).
[14]J. B. Lonzaga, "Recent enhancements to NASA's PCBoom sonic boom propagation code," in AIAA paper, AIAA 2019-3386 (2019).
[15]T. A. Stout, V. W. Sparrow, and P. Blanc-Benon, "Evaluation of numerical predictions of sonic boom level variability due to atmospheric turbulence," J. Acoust. Soc. Am. **149**, 3250–3260 (2021).
[16]F. Dagrau, M. Rénier, R. Marchiano, and F. Coulouvrat, "Acoustic shock wave propagation in a heterogeneous medium: A numerical simulation beyond the parabolic approximation," J. Acoust. Soc. Am. **130**(1), 20–32 (2011).
[17]J. Qiao, Z. Han, L. Zhang, W. Song, and B. Song, "Far-field sonic boom prediction considering atmospheric turbulence effects: An improved approach," Chin. J. Aeronaut. **35**(9), 208–225 (2022).
[18]M. Kanamori, T. Takahashi, Y. Makino, Y. Naka, H. Takahashi, and H. Ishikawa, "Numerical evaluation of sonic boom deformation due to atmospheric turbulence," AIAA J. **59**(3), 972–986 (2021).
[19]J. B. Lonzaga, "Multiple scattering theory for modeling sonic booms in atmospheric turbulence," J. Acoust. Soc. Am. **154**(5), 3078–3088 (2023).
[20]P. Blanc-Benon, B. Lipkens, L. Dallois, and M. F. Hamilton, "Propagation of finite amplitude sound through turbulence: Modeling with geometrical acoustics and the parabolic approximation," J. Acoust. Soc. Am. **111**(1), 487–498 (2002).
[21]P. V. Yuldashev, S. Ollivier, M. M. Karzova, V. A. Khokhlova, and P. Blanc-Benon, "Statistics of peak overpressure and shock steepness for linear and nonlinear N-wave propagation in a kinematic turbulence," J. Acoust. Soc. Am. **142**, 3402–3415 (2017).
[22]P. B. C. Leal, J. A. Schrass, T. N. Giblette, D. F. Hunaker, H. Shen, T. S. Logan, and D. J. Hartl, "Effects of atmospheric profiles on sonic boom perceived level from supersonic vehicles," AIAA J. **59**(12), 5020–5028 (2021).
[23]J. Salamone, "Recent sonic boom propagation studies at Gulfstream aerospace," in *Conference Proceedings of 15th AIAA/CEAS Aeroacoustics Conference*, AIAA 2009-3388 (2009).
[24]R. Blumrich, F. Coulouvrat, and D. Heimann, "Variability of focused sonic booms from accelerating supersonic aircraft in consideration of meteorological effects," J. Acoust. Soc. Am. **118**(2), 696–706 (2005).
[25]R. Blumrich, F. Coulouvrat, and D. Heimann, "Meteorologically induced variability of sonic-boom characteristics of supersonic aircraft in cruising flight," J. Acoust. Soc. Am. **118**, 707–722 (2005).
[26]D. Heimann, "Effects of long-term atmospheric variability on the width of a sonic-boom carpet produced by high-flying supersonic aircraft," Acoust. Res. Lett. Online **2**, 73–78 (2001).
[27]J. Takeno, T. Misaka, K. Shimoyama, and S. Obayashim, "Analysis of sonic boom propagation based on the KZK equation," in *Conference Proceedings of 53rd AIAA Aerospace Sciences Meeting*, AIAA 2015-0745 (2015).
[28]Y.-S. Lee, "Numerical solution of the KZK equation for pulsed finite amplitude sound beams in thermoviscous fluids," Ph.D. dissertation, University of Texas at Austin, Austin, TX, 1993.
[29]R. O. Cleveland, M. F. Hamilton, and D. T. Blackstock, "Time-domain modeling of finite-amplitude sound in relaxing fluids," J. Acoust. Soc. Am. **99**, 3312–3318 (1996).
[30]M. Kanamori, T. Takahashi, Y. Makino, Y. Naka, and H. Ishikawa, "Comparison of simulated sonic boom in stratified atmosphere with flight test measurements," AIAA J. **56**(7), 2743–2755 (2018).
[31]H. R. Welge, J. Bonet, T. Magee, D. Chen, S. Hollowell, A. Kutzmann, A. Mortlock, J. Stengle, C. Nelson, E. Adamson, S. Baughcum, R. T. Britt, G. Miller, and J. Tai, "N+2 supersonic concept development and systems integration," in *NASA/CR-2010-216842* (2010).
[32]T. E. Magee, S. G. Shaw, and S. R. Fugal, "Experimental validations of a low-boom aircraft design," in *Conference Proceedings of 51st AIAA Aerospace Sciences Meeting Including the New Horizons Forum and Aerospace Exposition*, AIAA 2013-0646 (2013).
[33]F. H. Grover, "Geophysical effects of Concorde sonic boom," Q. J. R. Astron. Soc. **14**, 141–158 (1973).
[34]H. Ishikawa, Y. Makino, K. Yoshida, and K. Ohira, "Sonic-boom analysis of a Concorde type airplane using the structured/unstructured overset grids method," in *Proceedings of JAXA-SP-10-012* (2011).
[35]H. Ishikawa, D. Y. Kwak, and K. Yoshida, "Numerical analysis on flight-test results of supersonic experimental airplane NEXST-1," J. Aircr. **45**(5), 1505–1514 (2008).
[36]P. Jöckel, A. Kerkweg, A. Pozzer, R. Sander, H. Tost, H. Riede, A. Baumgaertner, S. Gromov, and B. Kern, "Development cycle 2 of the Modular Earth Submodel System (MESSy2)," Geosci. Model Dev. **3**(2), 717–752 (2010).
[37]E. Roeckner, R. Brokopf, M. Esch, M. Giorgetta, S. Hagemann, L. Kornblueh, E. Manzini, U. Schlese, and U. Schulzweida, "Sensitivity of simulated climate to horizontal and vertical resolution in the ECHAM5 atmosphere model," J. Clim. **19**(16), 3771–3791 (2006).
[38]D. P. Dee, S. M. Uppala, A. J. Simmons, P. Berrisford, P. Poli, S. Kobayashi, U. Andrae, M. A. Balmaseda, G. Balsamo, P. Bauer, P. Bechtold, A. C. M. Beljaars, L. van de Berg, J. Bidlot, N. Bormann, C. Delsol, R. Dragani, M. Fuentes, A. J. Geer, L. Haimberger, S. B. Healy, H. Hersbach, E. V. Hólm, L. Isaksen, P. Kållberg, M. Köhler, M. Matricardi, A. P. McNally, B. M. Monge-Sanz, J.-J. Morcrette, B.-K. Park, C. Peubey, P. de Rosnay, C. Tavolato, J.-N. Thépaut, and F. Vitart, "The ERA-Interim reanalysis: Configuration and performance of the data assimilation system," Q. J. R. Meteorol. Soc. **137**, 553–597 (2011).
[39]H. Yamashita, F. Yin, V. Grewe, P. Jöckel, S. Matthes, B. Kern, K. Dahlmann, and C. Frömming, "Newly developed aircraft routing options for air traffic simulation in the chemistry-climate model EMAC 2.53: AirTraf 2.0," Geosci. Model Dev. **13**(10), 4869–4890 (2020).
[40]I. Orlanski, "A rational subdivision of scales for atmospheric processes," Bull. Am. Meteor. Soc **56**(5), 527–530 (1975).
[41]J. Hinze, *Turbulence*, 2nd ed. (McGraw-Hill, New York, 1959), Chap. 3, pp. 175–320.
[42]H. Yamashita and S. Obayashi, "Sonic boom variability due to homogeneous atmospheric turbulence," J. Aircr. **46**(6), 1886–1893 (2009).
[43]W. Bechara, C. Bailly, and P. Lafon, "Stochastic approach to noise modeling for free turbulent flows," AIAA J. **32**(3), 455–463 (1994).
[44]Dryden Flight Research Center, "Sonic booms," in *NASA Facts FS-2003-11-016 DFRC* (2023).
[45]G. M. Jackson and H. G. Leventhall, "Calculation of the perceived level of noise (PLdB) using Stevens' method (MARK VIII)," Appl. Acoust. **6**(1), 23–34 (1973).
[46]S. S. Stevens, "Perceived level of noise by Mark VII and decibels (*E*)," J. Acoust. Soc. Am. **51**, 575–601 (1972).
[47]C. R. Bolander, D. F. Hunsaker, H. Shen, and F. L. Carpenter, "A procedure for the calculation of the perceived loudness of sonic booms," in *Conference Proceedings of AIAA Scitech 2019 Forum*, AIAA 2019-2091 (2019).
[48]M. Yamamoto, A. Hashimoto, T. Takahashi, T. Kamamura, and T. Sakai, "Long-range sonic boom prediction considering atmospheric effects," in *Conference Proceedings of Inter-Noise 2011* (2011).
[49]H. Akoglu, "User's guide to correlation coefficients," Turk. J. Emerg. Med. **18**, 91–93 (2018).
[50]D. E. Hinkle, W. Wiersma, and S. G. Jurs, *Applied Statistics for the Behavioral Sciences*, 5th ed. (Houghton Mifflin, Boston, 2003).
[51]K. A. Bradley, C. M. Hobbs, C. B. Wilmer, V. W. Sparrow, T. A. Stout, J. M. Morgenstern, K. H. Underwood, D. J. Maglieri, R. A. Cowart, M. T. Collmar, H. Shen, and P. Blanc-Benon, "Sonic booms in atmospheric turbulence (SonicBAT): The influence of turbulence on shaped Sonic booms," NASA Contractor Report NASA/CR–2020–220509 (2020).
[52]H. H. Hubbard and D. J. Maglieri, "Sonic boom signature data from cruciform microphone array experiments during the 1966-67 EAFB national sonic boom evaluation program," NASA Contractor Report NASA/CR-182027 (1990).
[53]A. D. Pierce, "Spikes on sonic-boom pressure waveforms," J. Acoust. Soc. Am. **44**(4), 1052–1061 (1968).
[54]D. J. Maglieri and V. E. Sothcott, "Summary of sonic boom rise times observed during FAA community response studies over a 6-month period in the Oklahoma City area," NASA Contractor Report NASA/CR-4277 (1990).
[55]M. Averiyanov, S. Ollivier, V. Khokhlova, and P. Blanc-Benon, "Random focusing of nonlinear acoustic *N*-waves in fully developed turbulence: Laboratory scale experiment," J. Acoust. Soc. Am. **130**(6), 3596–3607 (2011).
[56]A. N. Carr, J. B. Lonzaga, and S. A. E. Miller, "Numerical prediction of loudness metrics for N-waves and shaped sonic booms in kinematic turbulence," J. Acoust. Soc. Am. **151**, 3580–3593 (2022).